



Experimental study on seepage-induced concentrated leak erosion in sand under triaxial testing conditions

Xingxin Chen¹ · Minan Fang^{1,2} · Biao Li³ · Ali Rostami³ · Liqun Guo¹ · Qipeng Cai¹

Received: 21 July 2021 / Accepted: 8 December 2021 / Published online: 29 December 2021
© Saudi Society for Geosciences 2021

Abstract

Seepage-induced engineering geology disasters such as sinkholes, foundation pits, and road collapses have resulted in massive economic losses and serious casualties in recent decades, with a major mechanism involved being sand internal erosion. In this research, a novel flexible-wall triaxial test apparatus is developed based on the conventional triaxial device to simulate concentrated leak erosion in sand using artificial quartz sand soil samples. Erosion tests are performed under different hydraulic gradients to study the variations of eroded soil mass and permeability. The results indicate that by increasing the applied hydraulic gradient, the position of the sunken portion (where large quantities of quartz sand particles are missing) elevates in the sample. Furthermore, particle loss rate and permeability coefficient show major variations under different hydraulic gradients. As the hydraulic gradient increases, the erosion rate of quartz sand content increases significantly accompanied by an increase in permeability. However, the start-up time and the duration of soil mass erosion as well as the variation in the permeability coefficient decrease. This study provides valuable insight into the mechanisms coupling the stress state, hydraulic gradient, and concentrated leak erosion phenomenon in sand.

Keywords Sand erosion · Seepage · Hydraulic gradient · Triaxial test · Leakage hole size

Introduction

Seepage-induced accidents such as foundation pit collapse, road collapse, and gushing of water and sand into tunnels have resulted in massive economic loss and the endangerment of human life (Guo et al. 2019; Koltuk et al. 2019; Kwak et al. 2019; Qiu et al. 2020; Zhang et al. 2019). Internal erosion occurs when soil particles are separated from the soil matrix by water seepage, which is a major cause of the failure of hydraulic earthen structures (e.g., dams and embankments) (Skempton and Brogan 1994; Wan and Fell 2004; Liu et al. 2020; Zhang et al. 2020). Long-term internal

erosion in soils around defective sewer pipes can also induce sinkholes and initiate a series of catastrophic events including interruption to buried service lines, disruption to traffic, contamination of nearby natural water bodies, damage to highway profiles, and sometimes human fatalities (Indiketiya et al. 2019). Seepage erosion happens once groundwater flow reaches a critical velocity, as it moves soil particles and creates caves within the soil. On May 10, 2012, 41 sinkholes opened, damaging 143 houses, 8 factories, and 3 commercial buildings, in the southern suburbs of Liuzhou, Guangxi province, China (Jiang 2018). Due to the poor sealing performance of the tail of the shield machine, a sudden water and sand gushing accident occurred in the shield tunnel of Foshan Metro Line 2 in 2018, resulting in a catastrophic collapse of the tunnel and surrounding road. In 2019, due to heavy rainfall and leakage of sewage pipelines, the support between piles was severely ruptured and water seeped into the foundation pit of a building in Beijing, eventually causing a severe collapse incident. Another incident occurred the same year; approximately 375 m² of ground area collapsed due to water and sand gushing from the construction face of tunneling for the Guangzhou Metro line 1. Overall, such

Responsible editor: Zeynal Abiddin Erguler

✉ Biao Li
biao.li@concordia.ca

¹ School of Civil Engineering, Huaqiao University, Xiamen 361021, Fujian, China

² Fujian Geotechnical Engineering Investigation Institute Co., Ltd., Fuzhou 350108, Fujian, China

³ Department of Building, Civil & Environmental Engineering, Concordia University, Montreal, Quebec H3G 1M8, Canada

seepage-induced accidents are often difficult to detect, and the consequences are extremely severe.

The disastrous consequences of seepage-induced accidents cannot be underestimated. Scientific studies on these incidents have offered important guidelines for engineering applications and high research standards (Reddi et al. 2000; Liu et al. 2018; Bai et al. 2016; Bai et al. 2019). The mechanisms of internal erosion are deeply complex entailing many parameters and two types of internal erosion can be distinguished: suffusion and interface erosion. The suffusion process occurs when the fine particles of an internally unstable soil move within the constrictions between the coarse particles, without any reduction in the total specimen volume (Zhou et al. 2020; Zhang et al. 2020). Interface erosion can appear within cracks or be caused by concentrated leaks and is also called concentrated leak erosion (Hicher et al. 2017). Concentrated leak erosion tends to generate cavities in a soil body and results in substantial sinkholes or ground settlement. Rapid development and large soil loss are two characteristics of concentrated leak erosion, which often lead to massive economic losses and can result in casualties (Ermolin and Melnikov 2019; Gao et al. 2018; Wu et al. 2018). Various model tests have been performed in previous research studies to investigate the mechanisms involved in concentrated leak erosion-induced soil failures. Mukunoki et al. (2012) applied air pressure on top of a cylindrical soil sample, supplied water into the sample through a defected pipe, and observed the size and shape of cavity developed in the soil during the sand erosion process using X-ray CT. Guo et al. (2013) set the sand in a transparent square test chamber, and set the leakage hole on the side wall of the chamber, where the development of the soil erosion could be observed from the transparent side wall of the chamber. Sato and Kuwano (2015) adopted an apparatus similar to the one employed by Guo et al. (2013), and buried a cylinder in the sand in order to simulate a pipe and analyze the influence of underground structures on the development of erosion. Based on the two apparatuses mentioned above, Indiketiya et al. (2019) performed model tests whereby they applied a load on the surface of the sample, and simulated erosion and sinkhole development due to cyclic leakage through pipe cracks. Tian et al. (2020) investigated the critical fine contents of natural soil deposits beyond which the internal stability of the soil mix was markedly changed, leading to internal erosion. They developed a fixed-wall permeameter capable of detecting the critical hydraulic gradient of erosion initiation and collecting the cumulative eroded soil mass at a constant inflow rate. Generally, majority of previous studies on concentrated leak erosion use rectangular or cylindrical apparatuses with rigid walls to hold soil samples. Although the initial stress state of soil can be simulated by applying air pressure and/or mechanical force on top of the sample, the three-dimensional stress state in the actual situation of

the original formation (i.e., the in situ condition) cannot be simulated using the rigid walls when cavity formation occurs in the soil sample. Therefore, the development of a flexible wall apparatus capable of taking into consideration the actual stress state of soil is necessary for simulating the concentrated leak erosion mechanism. Previous studies on suffusion failure present numerous experiences employing flexible wall devices, from which some key features are worth mentioning. They mainly use the confining pressure control system of the triaxial apparatus, where the sample is placed in a rubber membrane, to allow for the simulation of the actual three-dimensional stress state of soil (Chang and Zhang 2013). In addition, some aspects of the sample cap, base of triaxial pressure chamber, and collection system have been improved. For example, to evenly inject the erosion water into the soil sample, the filter close to the sample cap is made of a glass ball or geo-textile combined with a porous sieve plate (Bendahmane et al. 2008; Marot et al. 2016). In order to reduce the resistance of soil and water mixture in the pipeline, the channel at the base of the triaxial pressure chamber is expanded by being hollowed out to form a funnel-shaped cavity (Ke and Takahashi 2014; Xiao and Shwiyhat 2012). To accurately measure the quality of soil erosion, some studies applied optical sensors to improve the sensitivity of measuring device to the number of fine particles in the instrument (Ke and Takahashi 2014). However, above mentioned test apparatuses used for suffusion tests are only suitable for situations with a slight loss of fine particles and with a low seepage rate. Thus, they cannot be applied to study the concentrated leak erosion in sand where a leakage with high-quantity eroded particles occurs. Therefore, the existing flexible wall erosion test apparatus needs more improvements to become applicable for studying concentrated leak erosion processes.

In this study, a novel triaxial apparatus is proposed and fabricated based on the conventional triaxial device, in order to simulate the three-dimensional stress state of soil which allows the examination of the concentrated leak erosion mechanism in sand. The novel triaxial apparatus is comprised of a water supply system, a confining pressure control system, a triaxial pressure chamber system, and a collection system. The confining pressure control system simulates the stress state of the soil, the water supply system maintains the long-term stability of the erosion head, the triaxial pressure chamber system simulates the failure mechanism of sand erosion, and the collection system (with the characteristics of automatic separation of solid-liquid) implements the precise measurement of the erosion amount and the permeability coefficient. The apparatus is employed to perform tests under four different hydraulic gradients. The results of these sand erosion tests demonstrate enhanced particle loss rate and permeability coefficient in the sandy soil sample, caused by applying different hydraulic gradients.

These results provide valuable insight into the mechanisms that couple the stress state, hydraulic gradient, and internal erosion phenomenon.

Experimental methods and materials used

Description of the test apparatus

This apparatus is developed based on the conventional triaxial test device and is capable of simulating sand internal erosion with high precision. The test apparatus is comprised of four parts: water supply system (I), confining pressure control system (II), triaxial pressure chamber system (III), and collection system (IV), as shown in Figs. 1 and 2. High-precision pressure regulating valves are used in the testing system to guarantee a high-precision measurement. Before the test, a calibration on the pressure measurement was conducted to make sure the relative error is within 0.1%.

The water supply system (I) is composed of an air compressor capable of applying a maximum pressure of 500 kPa, a water storage tank with a maximum volume of 100 L, and a high-precision pressure regulating valve with a maximum error of 0.1 kPa, which can provide constant pressure erosion water flow with pressure values ranging from 0 to 500 kPa. For performing internal erosion tests on soil samples under different hydraulic gradients, it is critical to ensure that the test device can maintain a stable erosion head over a significant time period. The common peristaltic pump or

screw pump available in the domestic market cannot meet the requirements of the long-term steady flow condition, because the output pressure of these pumps is affected by the internal resistance of the soil sample. In this study, an air source with a stable pressure output is economically set up by combining an air compressor with a high-precision pressure regulating valve. After injecting compressed air into the sealed water storage tank, the water in the tank is supplied to the top of the sample under the air pressure. Here, the water pressure can be further regulated by another high-precision pressure regulating valve to provide the long-term stability of the erosion water pressure on top of the soil sample.

The confining pressure control system (II) is comprised of an air compressor with a maximum pressure of 500 kPa, a water storage tank with a maximum volume of 20 L, a high-precision pressure regulating valve with a maximum error of 0.1 kPa, and the confining pressure control system of a conventional triaxial test device which has a maximum pressure of 500 kPa. The system can provide two different confining pressure control systems that are linked with the triaxial pressure chamber system through a three-way valve. The first confining pressure control system is composed of an air compressor, a water storage tank, and a high-precision pressure regulating valve, which can keep the confining pressure stable regardless of the deformation values of the soil sample. This system has a maximum pressure of 500 kPa and a maximum error of 0.1 kPa. When the sample's volume changes significantly, the confining pressure applied by the air compressor is instantly restored to the set value

Fig. 1 Schematic of the novel triaxial test apparatus for simulating sand internal erosion

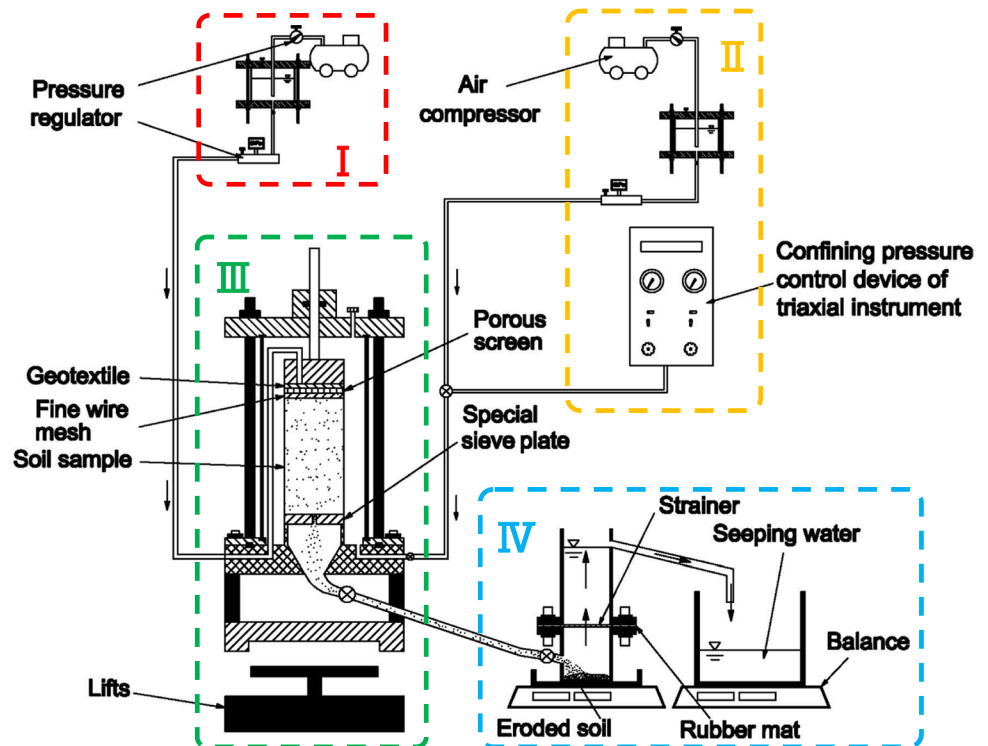
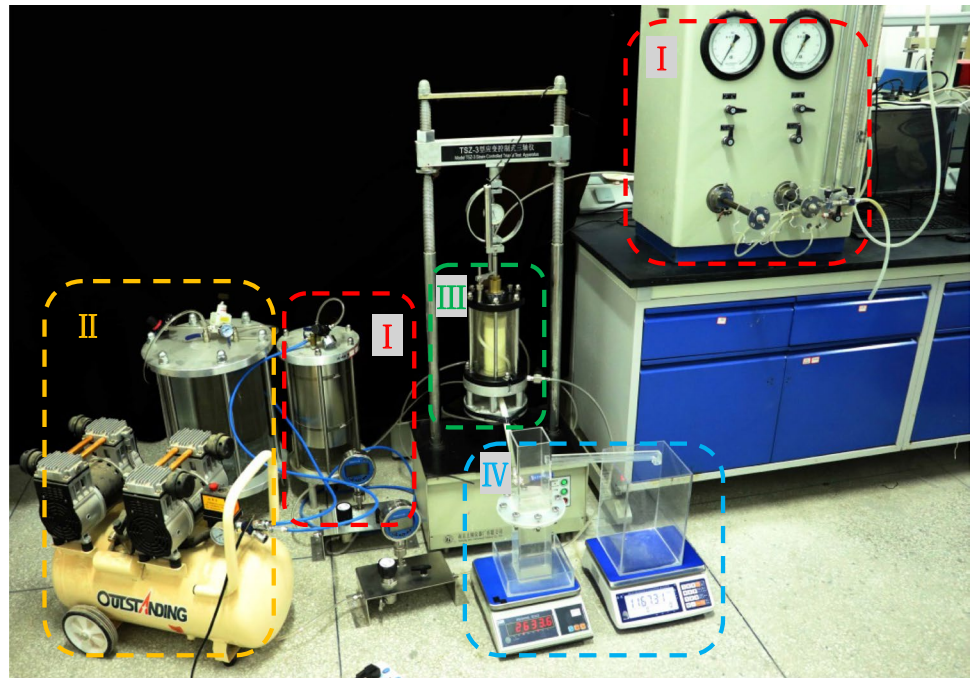


Fig. 2 Picture showing different parts of the novel triaxial test apparatus for simulating sand internal erosion



of the test. The purpose of this mechanism is to simulate a situation where underground soil with an erosion cavity is quickly filled by the surrounding soil due to the high surrounding pressure. The second confining pressure control system directly uses the conventional triaxial test device. The system has a maximum pressure of 500 kPa and a maximum error of 0.5 kPa. When the sample's volume reduces, for example by 10 mL, the confining pressure drops sharply and approaches zero, and the system requires a reaction time to compensate the pressure drop. This confining pressure control mechanism is suitable for situations where the underground soil experiences low surrounding pressure and thus the erosion cavity cannot be filled. In this regard, the soil in which an erosion cavity has occurred is identified as no longer being able to bear the surrounding pressure.

The triaxial pressure chamber system (III) is based on the pressure chamber of the conventional triaxial test device, mainly for three parts: sample cap, triaxial pressure chamber, and the base of triaxial pressure chamber. The cylindrical soil sample is set in a sealed rubber film so that the surrounding pressure can be properly applied to the soil during the test. The key feature of the pressure chamber system is that the soil in the effluent can be discharged smoothly, without blocking the pipeline, as the sand erosion occurs. Obviously, the permeable stone and pipelines of the conventional triaxial test device cannot meet the requirements of the sand erosion test. The triaxial pressure chamber system adopts a special sieve plate with a central hole, with diameter ranging from 0.5 to 20 mm, at the bottom of the soil sample which is appropriate for simulating different crack sizes of sand erosion. A

drainage pipeline with an overall diameter of 30 mm is adopted, connecting the triaxial pressure chamber and collection systems. This minimizes any chance for blockage of the pipeline throughout the entire sand erosion process.

The collection system (IV) consists of a solid–liquid separation apparatus, a liquid storage tank, and two high-resolution digital balances. The specially designed collection system is also used to increase the precision of the measurement. It separates the soil–water mixture discharged from the triaxial pressure chamber system, as well as monitors the quality of soil in the effluent and the permeability coefficient of the sample. The solid–liquid separation of the soil–water mixture is an important prerequisite for the observation of sand erosion test data. Unlike the previous collection systems, this collection system adopts a plexiglass tube with a diameter of 150 mm and corresponding filter screen with a relatively large diameter, which separates the soil particles from water. Furthermore, this system reduces the filtration resistance produced by the filter screen, economically achieves the soil–liquid separation, and obtains the test results with continuity and accuracy. The soil particles are prevented from passing through the filter screen and being deposited in the lower part of the solid–liquid separation device, while the water is collected in the liquid storage tank. The solid–liquid separation apparatus and the liquid storage tank are weighed in real time via the electronic balance, and the mass of soil particles and permeability coefficient can be calculated using the corresponding mathematical formula.

Characteristics of the test apparatus

The novel triaxial test apparatus has four unique characteristics exhibited by the four systems, which can be used for the experimental study of sand internal erosion mechanism. These characteristics are as follows:

- (1) To simulate the sand internal erosion under different stress conditions, this apparatus has two sets of confining pressure control systems. The first set is used to simulate the underground soil with high surrounding pressure, where the erosion cavity is quickly filled by the surrounding soil due to this high pressure. During the test, the system can maintain the stability of the confining pressure. The second set is utilized to simulate the underground soil experiencing low surrounding pressure, where the erosion cavity is not filled due to the low surrounding pressure. The soil in which an erosion cavity has already occurred can be regarded as a soil no longer capable of bearing the surrounding pressure.
- (2) A water supply system with stable output water pressure is developed. Air pressure is applied to the water storage tank through the air compressor. The output air pressure of the air compressor and the output water pressure of the water storage tank are controlled by the pressure regulating valves to maintain the stability of the erosion head and solve the problem of unstable output water pressure which exists with conventional water pumps.
- (3) The triaxial pressure chamber system adopts a special sieve plate that can simulate different leakage crack sizes, and an expanding drainage pipeline which minimizes any chance for blockage during the entire internal erosion process.
- (4) A new solid–liquid separation apparatus that can automatically separate the soil–water mixture discharged from the triaxial pressure chamber system, as well as monitor the quality of soil in the effluent and the permeability (coefficient) variation of the sample economically, efficiently, and accurately.

Calculation of erosion amount

The erosion amount can be characterized by the mass of solid soil discharged from the triaxial pressure chamber system, which is measured using the electronic balance. This requires that the soil solid and the water are effectively separated, which is implemented via the solid–liquid separation apparatus employed in this study.

According to the principle of erosion calculation, when the soil–water mixture is discharged into the solid–liquid separation device, the soil is deposited at the bottom of the

device. As the solid–liquid separation apparatus is filled with water, with the entry of a certain volume of eroded soil, the same volume of water flows out of the separation apparatus through the overflow port and into the liquid storage tank (Fig. 1). Based on the principle of mass balance, the formulation for the calculation of eroded soil mass is deduced as follows:

Assume that at time t_1 , the total mass of the solid–liquid separation device is M'_1 , and its mathematical expression is

$$M'_1 = M_{g1} + M'_{w1} + M'_s = M_{g1} + \rho_w(V - V'_s) + \rho_s V'_s \quad (1)$$

where M_{g1} is the mass of the solid–liquid separation device, M'_{w1} is the mass of water in the solid–liquid separation device at t_1 , M'_s is the mass of soil in solid–liquid separation device at t_1 , V is the volume of separation device, V'_s is the volume of soil in the separation device at t_1 , ρ_w is the density of water, and ρ_s is the density of soil.

Now, assume that at time t_2 , the total mass of the solid–liquid separation device is M''_1 , and its mathematical expression is

$$M''_1 = M_{g1} + M''_{w1} + M''_s = M_{g1} + \rho_w(V - V''_s) + \rho_s V''_s \quad (2)$$

where M''_{w1} is the mass of water in the solid–liquid separator at t_2 , M''_s is the mass of soil in the solid–liquid separator at t_2 , and V''_s is the volume of soil in the solid–liquid separator at t_2 .

Subtracting Eq. (1) from Eq. (2) yields

$$\Delta V_s = V''_s - V'_s = \frac{M''_1 - M'_1}{\rho_s - \rho_w} \quad (3)$$

where ΔV_s is the volume of soil discharged by the sample erosion in the (t_1-t_2) time period. By multiplying Eq. (3) and soil density, the mass m of the eroded soil in this time period can be obtained as

$$m = \rho_s \Delta V_s = \rho_s \frac{M''_1 - M'_1}{\rho_s - \rho_w} \quad (4)$$

Experimental procedure

Previous studies mainly used quartz sand, which exists abundantly in nature, as the material for the experimental study of sand internal erosion mechanism (Guo et al. 2013; Gao et al. 2018). Similarly, in this study, quartz sand soil samples are fabricated and prepared in layers by applying uniform compaction. The soil sample has a diameter of 61.8 mm and a height of 125 mm, and is placed in the apparatus within a sealed rubber film, then is subjected to a confining pressure of 100 kPa. The magnitude of applied confining pressure is to simulate the in-situ stress condition in a sand formation

surrounding a pipe with a buried depth of 5 m (Jung and Sinha 2007). The physical and mechanical parameters are presented in Table 1. The sand sample has a compaction coefficient of 80% meaning that the soil has been compacted to 80% of the maximum density achieved in the lab. Under such compaction condition, the soil sample has a void ratio of 0.71. The grading curve of studying sand soil sample is shown in Fig. 3, which indicates a median particle diameter of 0.1 mm. The diameters of a major of sand particles fall into the range of 0.1 to 0.3 mm. This type of poorly grade sand is usually used as a bedding material for buried pipes (Indiketiyi et al. 2019). The purpose of our concentrated leaking tests is to simulate a situation where the bedding material is subjected to a concentrated leaking due to the pipe damage.

A special plexiglass plate with a central hole is set at the bottom of the sample to simulate the soil sample being subject to the concentrated leakage of sand erosion. We have carried out tests with different central hole sizes to address the impact of leakage hole size on erosion results. Tests were arranged in three groups according to the leakage hole size (Table 2). Four hydraulic gradients (16, 24, 32, and 40) were applied to each group of tests to study the effect of different hydraulic gradients on sand erosion process. The applied

Table 1 Main physical and mechanical parameters of the soil sample

Dry density	Relative density	Compaction coefficient	Specific gravity	Void ratio
ρ_d (g/cm ³)	D_r (%)	λ_c (%)	G_s	e_0
1.55	67	80	2.65	0.71

Fig. 3 Grain size distribution curve of the soil sample

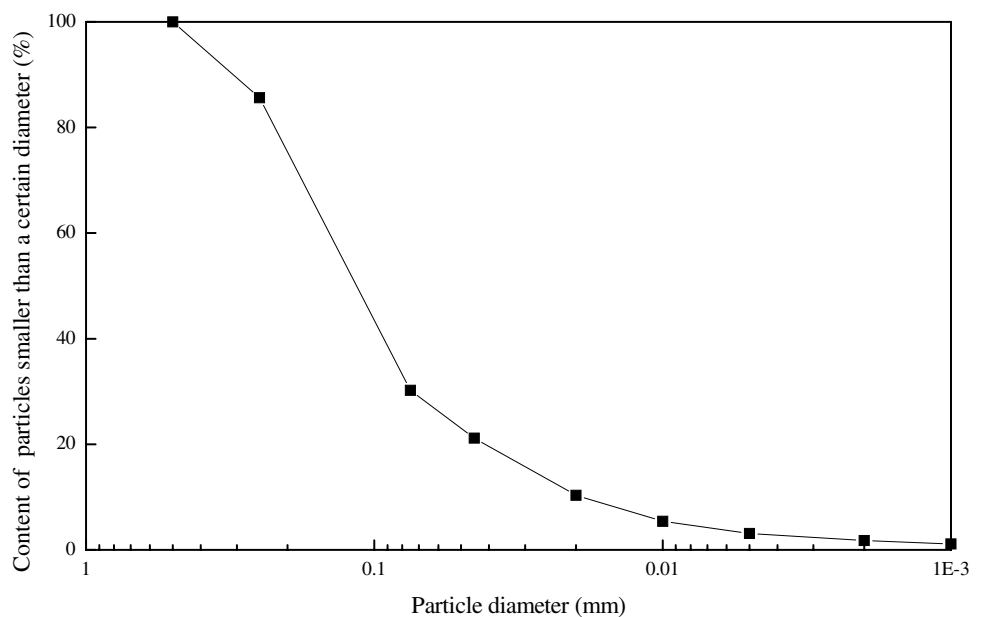


Table 2 A list of concentrated leak erosion tests conducted in this study

Test	Leakage hole size (mm)	Hydraulic gradient	Duration (min)
Group 1	2	16, 24, 32, 40	50, 40, 30, 32
Group 2	2.3	16, 24, 32, 40	41, 40, 29, 26
Group 3	2.6	16, 24, 32, 40	41, 30, 23, 22

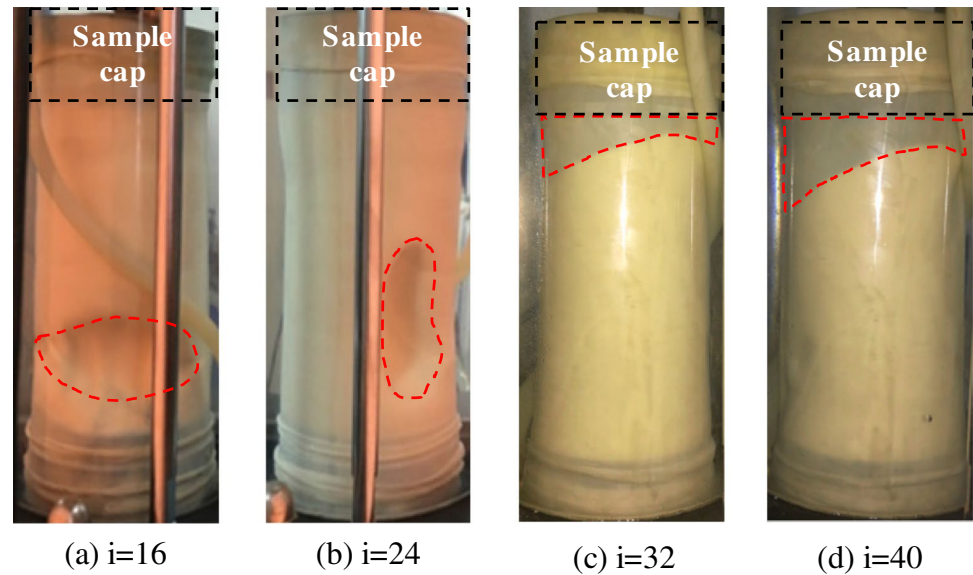
high hydraulic gradients are to simulate the high pore water pressure condition created during the leaking of a water supply pipe. During each test, the discharged quartz sand content and the permeability coefficient of the soil sample are monitored and measured. In addition, the changes in the outer surface of the sample, due to sand internal erosion, are recorded using a camera. This data demonstrates the effects of the applied hydraulic gradient on sand internal erosion mechanism and permeability variation.

Results and analysis

Qualitative description of internal erosion

Figure 4(a)–(d) show the side images of the soil samples from group 1 at $t = 2$ min after the sand erosion start-up. The areas enclosed by red dashed lines in Fig. 4 indicate sunken portions in the samples where large quantities of quartz sand are missing at the early stage of sand erosion. Figure 4 also shows that the position of the first sunken portion, where quartz sand particles are missing, gradually goes higher in the sample as the applied hydraulic gradient increases.

Fig. 4 Side photographs of soil samples at $t = 2$ min after the start-up of sand erosion ($i =$ hydraulic gradient)



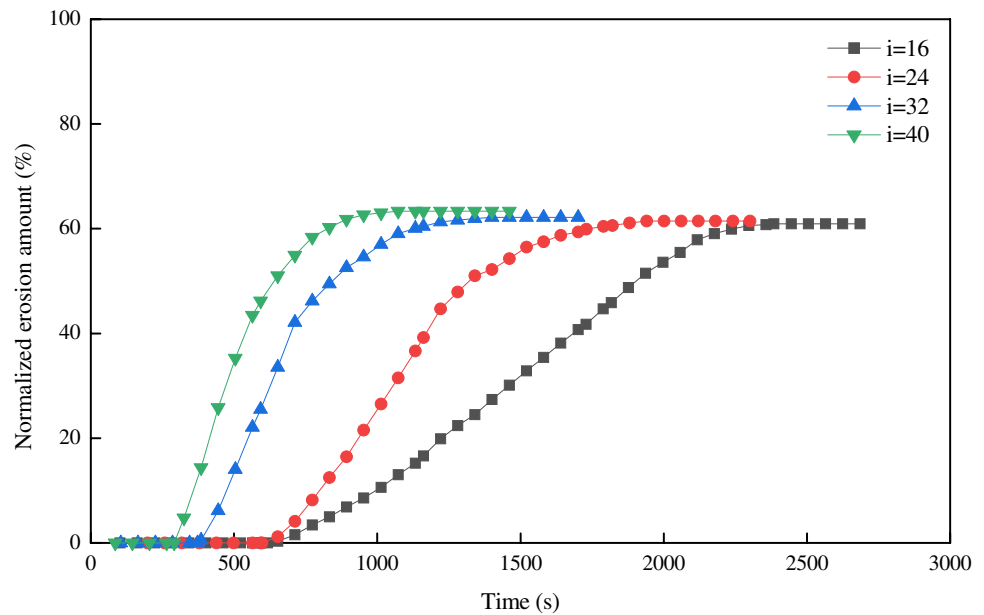
For instance, when the applied hydraulic gradient is 16, the sunken portion is in the lower part of the sample. Then, when the applied hydraulic gradient is 24, the position of the sunken portion elevates to the middle part of the sample. Finally, when the applied hydraulic gradients are at values of 32 and 40, the first sunken portion is located at the top of the soil sample. These observations indicate a close relation between the sunken portion and the hydrodynamic force within the soil sample. After the sand erosion commences, the (quartz sand) soil near the leakage holes discharges first, and cavities are generated from the inside of the sample. The soil arch structure, formed by these cavities, bears the vertical seepage force and the radial confining pressure. The hydrodynamic force typically increases with the increase of the hydraulic gradient. When the hydrodynamic force is small (i.e., under low values of hydraulic gradient), the radial part of the soil arch structure is damaged firstly. Thus, sand particles tend to migrate along the radial direction and result in an evident sunken portion in the lower part of the sample. However, when the hydrodynamic force is large (i.e., under high values of hydraulic gradient), the vertical part of the soil arch structure is the first to be damaged, and sand particles flow vertically into the cavity in a high speed. Therefore, a large number of quartz sand particles are lost in the upper part of the sample.

Mass loss mechanism in the sand internal erosion process

The amount of normalized erosion (as a function of time) for group 1 tests during the sand erosion process is illustrated in Fig. 5. In this figure, the normalized erosion amount refers to the ratio of the mass of quartz sand loss to the dry mass of the soil sample before the test. The erosion

amount of quartz sand in the soil sample follows a trend as the following. Before the sand erosion, the erosion amount is stable and almost equal to zero. As sand internal erosion begins the erosion amount rises sharply, and finally the erosion amount tends to stabilize. For instance, when the applied hydraulic gradient is 24, the erosion amount is equal to zero for the time period of 0 to 593 s, indicating the absence of sand erosion during this period. In the next time period ranging from 594 to 1340 s, the erosion mass ratio of sand erosion in the sample increases from 0 to 51.0%. Here, the erosion amount shows a sharply increasing trend, indicating a period of rapid development of sand erosion. During the third time period ranging from 1341 to 1730 s, the erosion amount increases from 51.0 to 59.9%, showing that the rate of increase of the erosion amount has reduced greatly and the sand erosion is reaching completion. Finally, within the last time period ranging from 1731 to 2300 s, the erosion amount of the soil essentially does not change, indicating that the sand erosion has ceased. To be more specific, the soil sample is subject to both hydrodynamic force and confining pressure simultaneously. On one hand, the soil bears a downward hydrodynamic force, which causes the quartz sand in the sample to move downward and run off from the leakage hole which promotes cavity generation. On the other hand, the soil is subject to a confining pressure, causing the radial migration of sand particles. In the early stage of sand internal erosion, both hydrodynamic force and confining pressure are constant. Under their combined action, the erosion amount of the soil sample shows a sharply increasing trend. After the early stage of sand erosion, the soil sample experiences a large volume of shrinkage due to the gradual increase in the amount of quartz sand loss, and the confining pressure is reduced due to the slow rate of pressurization supplied

Fig. 5 Normalized erosion amount as a function of time at different hydraulic gradients



by the confining pressure control system (as explained earlier). This causes the quartz sand loss to slow down, which consequently lowers the rate of sample erosion. During the next stage of sand erosion, the sample is essentially no longer subjected to the confining pressure, and the quartz sand particles only bear the effect of the hydrodynamic force. As a result, a stable water passage at the leakage hole is formed, so the quartz sand particles do not migrate. Therefore, the sample's erosion amount does not change. Overall, the sand erosion process of the quartz sand in the sample is rapid and transient, which is mainly attributed to the low cohesion of the quartz sand sample.

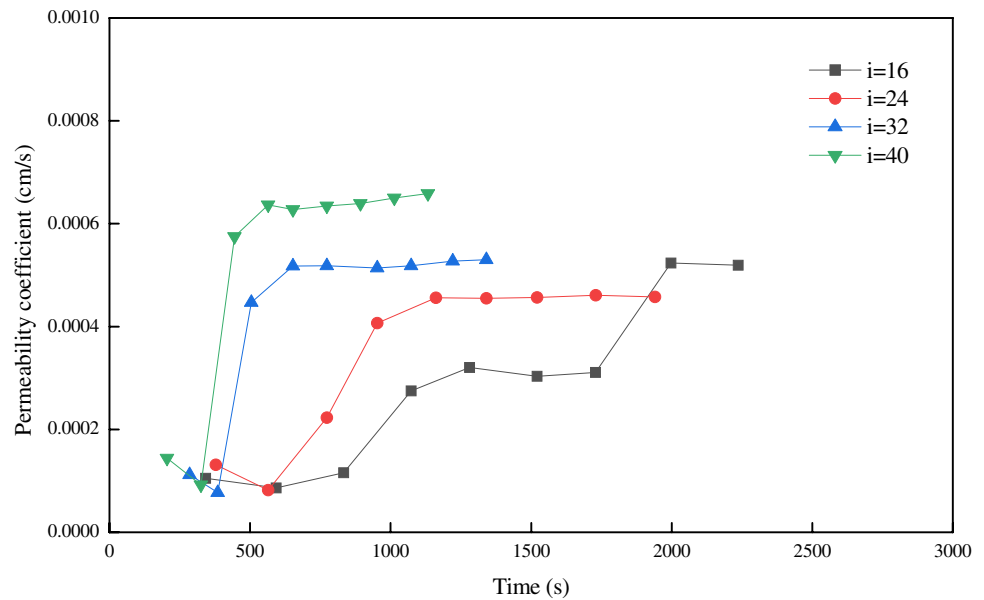
A comparison of the curves shown in Fig. 5 (i.e., Normalized erosion amount vs. Time) indicates that by increasing the hydraulic gradient, the starting time and the duration of sand erosion decrease. However, the final total loss of quartz sand particles under the four different hydraulic gradients is almost the same. For the applied hydraulic gradients of 16, 24, 32, and 40, the starting times of the sand erosion are 653 s, 593 s, 385 s, and 325 s, respectively, and the corresponding sand erosion durations are 1523 s, 1108 s, 688 s, and 953 s. The final total losses of quartz sand particles under these four different hydraulic gradients are around 61%. These observations confirm that the starting time and the duration of sand erosion are closely related to the hydrodynamic force in the soil sample. A larger hydraulic gradient result in a larger hydrodynamic force experienced by the soil sample; thus, an earlier erosion occurs to tests with larger hydraulic gradients. Furthermore, under a higher hydraulic gradient the corresponding rate of sand loss is higher, but it has a negligible effect on the final total loss in quantity.

Permeability changes in sand erosion process

Figure 6 shows the measured permeability coefficient of the sample as a function of time for tests from the group 1. Permeability coefficients were measured using the constant head approach (Das 1997). The variation trend of the permeability coefficient under each hydraulic gradient is similar to that of the normalized erosion amount shown in Fig. 5. For example, when the applied hydraulic gradient is 24, the permeability coefficient of the sample is approximately equal to 0.0001 cm/s for the time period of 0 to 565 s, then it increases to 0.0004 cm/s for the next time period ranging from 566 to 1161 s, and it remains stable at the approximate value of 0.0004 cm/s for the third time period ranging from 1162 to 1941 s. Despite the variation trends of the permeability coefficient and the erosion amount being consistent with each other, the change in the permeability coefficient appears to start approximately 30 s before the change in the erosion amount begins. This is mainly because the loss of sand particles, which is transported from the bottom of the triaxial pressure chamber system to the collection system, needs to pass through a pipe (of a certain length) and results in a delay of 30 s.

A comparison of the curves shown in Fig. 6 indicates that as the applied hydraulic gradient increases, the start-up time and the duration of variation in the permeability coefficient decrease. For the applied hydraulic gradients of 16, 24, 32, and 40, the start-up times are 833, 565, 385, and 325 s, respectively, and their corresponding durations are 1164, 596, 268, and 240 s. The variation trend of the sample's permeability is closely related to the variation trend of the quartz sand erosion amount.

Fig. 6 Permeability coefficient as a function of time at different hydraulic gradients



As the hydraulic gradient increases, the erosion rate of quartz sand increases and creates a larger void space for fluid flow; thus, the sample's permeability increases accordingly. It should be noted the loss of mass leads to a reduction in the height of the sample (Fig. 4), which is significant for cases of $i = 32$ and $i = 40$. Our calculation of hydraulic gradient will not be accurate in the late stage of erosion due to the change in sample heights. Thus, measured permeability changes are to some extent exaggerated. In order to obtain more accurate permeability results, sample size calibrations should be carried out for these erosion tests.

Effect of leakage hole size on sand erosion process

Previous results on group 1 were based on tests with a leakage hole size $d = 2.3$ mm. We also carried out some tests with leakage hole sizes of 2 mm and 2.6 mm (groups 2 and 3) to investigate the impact of leakage hole size on sand erosion processes. The developments of normalized sand erosion amount for cases with different leakage hole sizes and hydraulic gradients are displayed in Fig. 7(a)–(d). In general, the ultimate erosion amount is dependent on the leakage hole size. The leakage amounts for cases with a hole size of 2 mm are much lower than cases with hole sizes of 2.3 mm and 2.6 mm. Under a low hydraulic gradient (Fig. 7a), the sand erosion amounts vary significantly for cases with different leakage hole sizes in terms of the time to achieve a stable level. However, under a high hydraulic gradient (Fig. 7d), the difference between cases of 2.3 mm and 2.6 mm is negligible.

Discussions

Comparison with suffusion tests

The poorly graded soil samples applied in this study were to simulate the uniform sand surrounding buried pipes as a bedding material. If a well-graded soil sample is used, the erosion process tends to generate suffusion, where fine particles migrate through and into the pore space formed by coarse particles and the erosion rate will be much slower. The suffusion tests conducted by Chang and Zhang (2013) are also based on modified triaxial tests, and the initiation and development of internal erosion of fine particles through the coarse soil particles are investigated. The migration of fine particles through the intergranular space of coarse particles does not require a high hydraulic gradient. In addition, during the initiation and development of a suffusion process, coarse soil particles still serve as the skeleton and maintain the stability of the soil sample. By contrast, in our concentrated leak erosion tests on poorly graded sand soil samples, the tests have a higher hydraulic gradient and sand particles tend to erode by a large quantity in a short testing period. Thus, the tests are more challenging to complete because samples tend to lose the integrity quickly, which brings the difficulties in data collection.

Scale effect and in situ condition

For tests with the same leakage hole size and hydraulic condition, sand samples with a larger particle mean size

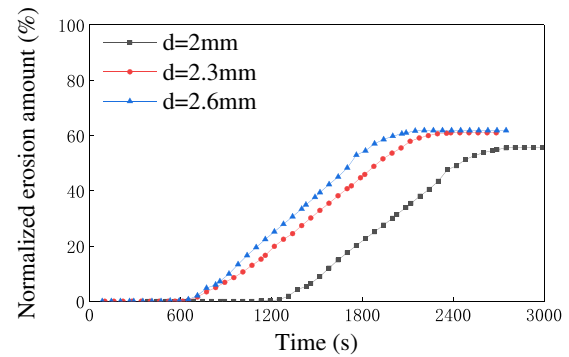
Fig. 7 Normalized erosion amount as a function of time for cases with different leakage hole sizes (d) and hydraulic gradients (i)

will not yield the same erosion amount. Thus, in engineering practical analysis, it is necessary to consider the relative sizes between leakage hole and sand particles. There will be a scale effect in the relative sizes. In addition, the triaxial experiment fundamentally simulates the uniform portion in the ground and the volume of the specimen is very limited and small. Therefore, the soil erosion is finished at the certain amount and the specimen membrane prevents the much more soil loss. Currently, there is a lack of in-situ data to interpret the mechanisms of field scale concentrated leak erosion in sand. An idea is to perform concentrated leak erosion tests on small-scale models installed in a geotechnical centrifuge. To interpret the test data, it will be necessary to quantify the scaling laws of the erosion phenomenon (Marot et al. 2012).

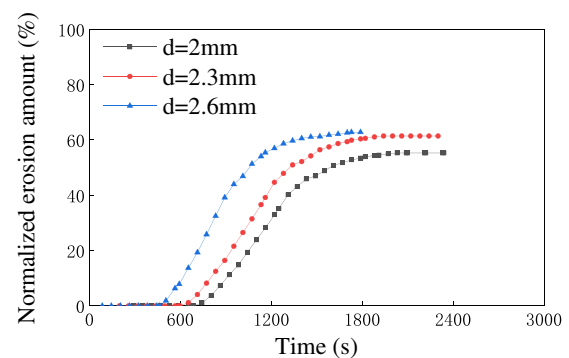
Conclusions

This study primarily introduces a novel experimental apparatus to simulate the concentrated leak erosion in sand. The system consists of a confining pressure control system, a water supply system, a triaxial pressure chamber system, and a collection system. Using the newly fabricated device, sand internal erosion tests are carried out under four different hydraulic gradients, where the erosion loss mechanism and the permeability variation are studied. The main conclusions are listed as follows:

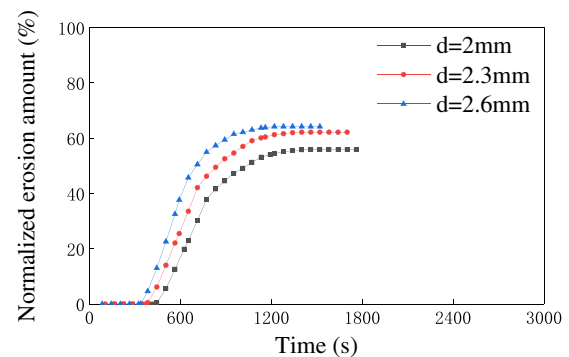
- (1) The newly developed triaxial test apparatus, for simulating the sand internal erosion mechanism, is economical, efficient, and accurate. The confining pressure control system simulates the sand internal erosion under different stress conditions. The water supply system maintains the long-term stability of the erosion head, and the particle collection system implements the automatic separation of soil particles and water discharged during the sand internal erosion process.
- (2) At a low hydraulic gradient, the radial part of the soil arch structure is damaged firstly, and the sand particles tend to flow into the cavity from the radial direction, resulting in a large amount of sand lost in the lower part of the sample. On the other hand, when the applied hydraulic gradient is high, the vertical part of the soil arch structure is primarily damaged, and sand particles flow into the cavity along the sample's axial direction, resulting in a large amount of particles lost in the upper part of the sample.
- (3) As the hydraulic gradient increases, the start-up time and the duration of sand internal erosion decrease.



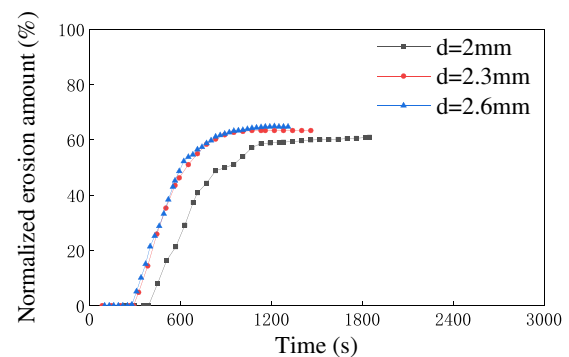
(a) $i = 16$



(b) $i = 24$



(c) $i = 32$



(d) $i = 40$

Despite this, eventually, the total loss of quartz sand content under the four different hydraulic gradients is almost the same. An increase in hydraulic gradient also leads to an increase in the permeability of the soil sample. The sand erosion amounts also vary significantly for cases with different leakage hole sizes in terms of the time to achieve a stable level.

Acknowledgements Comments from three anonymous reviewers are beneficial for this manuscript.

Availability of data and material Available upon request.

Code availability Not applicable.

Funding This research work was supported by the National Natural Science Foundation of China (NSFC) (grant numbers 51308235 and 51778249) and Concordia University Seed start up grant (No. VS1233).

Declarations

Conflict of interest The authors declare no competing interests.

References

- Bai B, Xu T, Guo Z (2016) An experimental and theoretical study of the seepage migration of suspended particles with different sizes. *Hydrogeol J* 24:2063–2078. <https://doi.org/10.1007/s10040-016-1450-7>
- Bai B, Rao D, Chang T, Guo Z (2019) A nonlinear attachment-detachment model with adsorption hysteresis for suspension-colloidal transport in porous media. *J Hydrol* 578:124080. <https://doi.org/10.1016/j.jhydrol.2019.124080>
- Bendahmane F, Marot D, Alexis A (2008) Experimental parametric study of suffusion and backward erosion. *J Geotech Geoenviron* 134(1):57–67. [https://doi.org/10.1061/\(ASCE\)1090-0241\(2008\)134:1\(57\)](https://doi.org/10.1061/(ASCE)1090-0241(2008)134:1(57))
- Chang DS, Zhang LM (2013) Critical hydraulic gradients of internal erosion under complex stress states. *J Geotech Geoenviron Eng, ASCE* 139(9):1454–1467
- Das BM (1997) *Advanced soil mechanics*. Taylor & Francis
- Ermolin E, Melnikov VN (2019) Gravity anomaly over the washout zone of the St. Petersburg Metro. *Engineering and Mining Geophysics 2019 15th Conference and Exhibition. European Assoc Geoscientists & Engineers* 2019(1):1–8. <https://doi.org/10.3997/2214-4609.201901789>
- Gao G, Yao S, Cui Y, Chen Q, Zhang X, Wang K (2018) Zoning of confined aquifers inrush and quicksand in Shanghai region. *Nat Hazards* 91(3):1341–1363. <https://doi.org/10.1007/s11069-018-3189-z>
- Guo X, Chai JR, Qin Y, Xu Z-G (2019) Mechanism and treatment technology of three water inrush events in the Jiaoxi River Tunnel in Shaanxi, China. *J Perform Constr Fac* 33(1):04018098. [https://doi.org/10.1061/\(ASCE\)CF.1943-5509.0001251](https://doi.org/10.1061/(ASCE)CF.1943-5509.0001251)
- Guo S, Shao Y, Zhang T, Zhu DZ (2013) Physical modeling on sand erosion around defective sewer pipes under the influence of groundwater. *J Hydraul Eng* 139(12):1247–1257. [https://doi.org/10.1061/\(ASCE\)HY.1943-7900.0000785](https://doi.org/10.1061/(ASCE)HY.1943-7900.0000785)
- Hicher PY, Marot D, Sibille L (2017) Chapter 9—internal erosion. F. Nicot & O. Millet. *Advances in Multi-Physics and Multi-Scale Couplings in Geo-Environmental Mechanics*, ISTE - Elsevier, pp. 291–334, 978-1-78548-278-6
- Indiketiya S, Jegatheesan P, Rajeev P, Kuwano R (2019) The influence of pipe embedment material on sinkhole formation due to erosion around defective sewers. *Transp Geotech* 19:110–125. <https://doi.org/10.1016/j.trgeo.2019.03.001>
- Jiang F (2018) Discussion of the pipe flow model to analyze the critical parameter of seepage erosion forming sinkholes in Liuzhou, China. *Bull Eng Geol Environ* 78:1417–1425. <https://doi.org/10.1007/s10064-017-1222-1>
- Jung YJ, Sinha SK (2007) Evaluation of trenchless technology methods for municipal infrastructure system. *J Infrastruct Syst* 13(2):144–156. [https://doi.org/10.1061/\(ASCE\)1076-0342\(2007\)13:2\(144\)](https://doi.org/10.1061/(ASCE)1076-0342(2007)13:2(144))
- Ke L, Takahashi A (2014) Experimental investigations on suffusion characteristics and its mechanical consequences on saturated cohesionless soil. *Soils Found* 54(4):713–730. <https://doi.org/10.1016/j.sandf.2014.06.024>
- Koltuk S, Song J, Iyisan R, Azzam R (2019) Seepage failure by heave in sheeted excavation pits constructed in stratified cohesionless soils. *Front Struct Civ Eng* 13(6):1415–1431. <https://doi.org/10.1007/s11709-019-0565-z>
- Kwak TY, Woo SI, Kim J, Chung C-K (2019) Model test assessment of the generation of underground cavities and ground cave-ins by damaged sewer pipes. *Soils Found* 59(3):586–600. <https://doi.org/10.1016/j.sandf.2018.12.011>
- Liu W, Zhao T, Zhou W, Tang J (2018) Safety risk factors of metro tunnel construction in China: an integrated study with EFA and SEM. *Saf Sci* 105:98–113. <https://doi.org/10.1016/j.ssci.2018.01.009>
- Liu W, Wan S, Luo X, Fu M (2020) Experimental study of suffusion characteristics within granite residual soil controlling inflow velocity. *Arab J Geosci* 13:1191. <https://doi.org/10.1007/s12517-020-06193-x>
- Marot D, Le VD, Garnier J, Thorel L, Audrain P (2012) Study of scale effect in an internal erosion mechanism: centrifuge model and energy analysis. *Eur J Environ Civ Eng* 16:1–19
- Marot D, Rochim A, Nguyen HH, Bendahmane F, Sibille L (2016) Assessing the susceptibility of gap-graded soils to internal erosion: proposition of a new experimental methodology. *Nat Hazards* 83(1):365–388. <https://doi.org/10.1007/s11069-016-2319-8>
- Mukunoki T, Kumano N, Otani J (2012) Image analysis of soil failure on defective underground pipe due to cyclic water supply and drainage using X-ray CT. *Front Struct Civ Eng* 6(2):85–100. <https://doi.org/10.1007/s11709-012-0159-5>
- Poesen J (2018) Soil erosion in the Anthropocene: research needs. *Earth Surf Proc Land* 43(1):64–84. <https://doi.org/10.1002/esp.4250>
- Qiu J, Lu Y, Lai J, Zhang Y, Yang T, Wang K (2020) Experimental study on the effect of water gushing on loess metro tunnel. *Environ Earth Sci* 79:1–19. <https://doi.org/10.1007/s12665-020-08995-4>
- Reddi LN, Lee IM, Bonala MVS (2000) Comparison of internal and surface erosion using flow pump tests on a sand-kaolinite mixture. *Geotech Test J* 23:116–122
- Sato M, Kuwano R (2015) Influence of location of subsurface structures on development of underground cavities induced by internal erosion. *Soils Found* 55(4):829–840. <https://doi.org/10.1016/j.sandf.2015.06.014>
- Skempton AW, Brogan JM (1994) Experiments on piping in sandy gravels. *Géotechnique* 44:449–460
- Tian D, Xie Q, Fu X, Zhang J (2020) Experimental study on the effect of fine contents on internal erosion in natural soil deposits. *Bull Eng Geol Environ*. <https://doi.org/10.1007/s10064-020-01829-4>
- Wan CF, Fell R (2004) Investigation of rate of erosion of soils in embankment dams. *J Geotech geoenvironmental Eng* 130:373–380

- Wu YX, Lyu HM, Shen SL, Arulrajah A (2018) Geological and hydro-geological environment in Tianjin with potential geohazards and groundwater control during excavation. *Environ Earth Sci* 77(10):392. <https://doi.org/10.1007/s12665-018-7555-7>
- Xiao M, Shwiyhat N (2012) Experimental investigation of the effects of suffusion on physical and geomechanic characteristics of sandy soils. *Geotech Test J* 35(6):890–900. <https://doi.org/10.1520/GTJ104594>
- Ye Z, Liu H (2020) Modeling the effects of internal erosion on the structural damage of a shield tunnel. *Int J Geomech* 20(6):04020053. [https://doi.org/10.1061/\(ASCE\)GM.1943-5622.0001691](https://doi.org/10.1061/(ASCE)GM.1943-5622.0001691)
- Zhang F, Li M, Peng M, Chen C, Zhang L (2019) Three-dimensional DEM modeling of the stress-strain behavior for the gap-graded soils subjected to internal erosion. *Acta Geotechnica* 14(2):487–503. <https://doi.org/10.1007/s11440-018-0655-4>
- Zhang F, Wang T, Liu F, Peng M, Furtney J, Zhang L (2020) Modeling of fluid-particle interaction by coupling the discrete element method with a dynamic fluid mesh: implications to suffusion in gap-graded soils. *Comput. Geotech.* 124:103617. <https://doi.org/10.1016/j.compgeo.2020.103617>
- Zhang G, Zhang K, Wang L, Wu Y (2014) Mechanism of water inrush and quicksand movement induced by a borehole and measures for prevention and remediation. *Bull Eng Geol Environ* 74(4):1395–1405. <https://doi.org/10.1007/s10064-014-0714-5>
- Zhou Z, Li Z, Ranjith PG, When Z, Shi S, Wei C (2020) Numerical simulation of the influence of seepage direction of suffusion in granular soils. *Arab. J. Geosci* 13:669. <https://doi.org/10.1007/s12517-020-05504-6>